5.2 GLOBAL DISTRIBUTION OF CONVECTION PENETRATING THE TROPICAL TROPOPAUSE

Chuntao Liu* and Edward J. Zipser
University of Utah, Salt Lake City, Utah

1. INTRODUCTION

Tropical cumulonimbus clouds have long been recognized not only to be essential to the global energy balance by transporting moist static energy to upper troposphere, but also by playing important role on global circulation and mass exchange between troposphere and stratosphere. Some recent theoretical studies, e.g. Sherwood and Dessler [2000] suggest that these clouds may have a major impact on the Tropical Tropopause Layer (TTL) water vapor budget.

The motivation of this study is to use a large satellite remote sensing database to quantify the properties of convective systems reaching the TTL. In the following sections, the size, overshooting area, volume and ice mass, geo-distribution and seasonal variations of convection with overshooting tops are quantitatively investigated with 5 years of Tropical Rainfall Measuring Mission (TRMM) [Simpson et. al. 1988, Kummerow et al. 1998] data using the Utah TRMM precipitation feature database.

2. DATA AND METHODOLOGY

5 years of TRMM precipitation radar (PR) measured reflectivity from Jan 1998 to Nov 2000 and from Dec 2001 to Dec2003 are grouped into precipitation features (PFs) with adjacent pixels greater than 20 dBZ using the method described by Nesbitt et al [2000]. More than 5 million PFs were found in 20^oN-20^oS tropical region. Then the environment sounding for each one of these PFs are obtained by interpolation from 2.5^o x 2.5^o, 6 hour interval NCEP reanalysis data described by Kistler et al [2001]. After recording the general information of PF size (total pixel numbers), mean rain rate, convective rain contribution etc., the convective intensity proxies including minimum TRMM Microwave Imager (TMI) 85 GHz Polarization Corrected Temperature (PCT) [Spencer et al., 1989], the maximum heights of PR 20 and 40 dBZ, maximum PR reflectivity at 6 and 9 km and flash counts observed by TRMM Lightning Imaging Sensor (LIS) for each PF are analyzed.

To find the PFs with overshooting tops, a definition of reference height is required. In addition to the 14 km used by Alcala and Dessler [2002], four different reference heights are defined and used here: level of NCEP reanalysis tropopause (Z_{trop}), level of potential temperature equal to 380 K (Z_{380K}) calculated from the NCEP sounding, Level of Neutral Buoyancy (LNB) calculated using NCEP sounding and surface equivalent potential temperature (LNB_{sfc}) and Level of Neutral Buoyancy calculated using equivalent potential temperature at 925 and 1000 mb, whichever is greater ($LNB_{925\&1000}$). Then, the Overshooting PFs (OPFs) are defined when the maximum height of the 20 dBZ echo exceeds14 km or any of the other defined reference heights, respectively.

The overshooting area of each OPF is calculated by multiplying the number of overshooting pixels with more than 20 dBZ at the reference height with the pixel size (~17.92 km^2 before the satellite orbit change and ~20.35 km^2 after the orbit boost). In addition to overshooting area, the overshooting volume and precipitating ice mass for each OPF are calculated as well. The overshooting volume of each OPF is calculated by summing all pixels above the reference heights with reflectivity > 20 dBZ and multiplying by the unit volume of each pixel (~4.48 km^3 before the satellite orbit change and ~5.09 km^3 after the orbit boost). The overshooting mass is calculated by integrating the precipitating ice mass of pixels above the reference level. The precipitating ice mass of each pixel is estimated using the Z-M_{ice} relation described by Carey and Rutledge [2000].

Population, mean overshooting distance, and overshooting area of the identified OPFs are listed in Table 1. While 1.38% of PFs have 20 dBZ echo to 14 km, only 0.1% of PFs were found reaching level of 380 K. On average, ~8% of OPF raining area detected by the PR has overshooting above 14 km from these OPFs, which is only 0.023% of the total PR sample area. When higher reference heights are used, the PFs tend to have larger overshooting area and smaller raining area – indicating that as the definition is more restrictive to the very tallest and strongest storms, they may be at an earlier stage of their life cycle , or isolated severe convective storms that may not ever evolve into mesoscale convective systems (MCSs). Comparing with the figure of ~0.5% overshooting area in the tropics reported by Gettelman et al. [2002], only 0.008% of our total sample area has a 20 dBZ echo above the NCEP tropopause.

Table 1. Population, overshooting distance, and area of overshooting precipitation features (OPFs) identified with respect to 5 definitions of reference heights.

Reference heights	14 km	LNB_{sfc}	$LNB_{925\&1000}$	Z_{trop}	Z_{380K}
OPFs population (#)	71989	28011	30355	9641	5512
Population percentage (%)	1.38	0.54	0.58	0.19	0.11
Mean reference height (km)	14.00	14.55	14.74	16.31	16.83
Mean Z_{20dBZ} (km)	15.34	15.68	15.79	16.98	17.44
Mean overshooting distance (km)	1.34	1.14	1.04	0.67	0.61
Mean OPFs overshooting area (km^2)	244	288	316	595	722
Mean overshooting area / OPF raining area (%)	8.19	8.96	9.31	13.51	15.85
Total overshooting area / total raining area (%)	0.58	0.27	0.32	0.19	0.13
Total overshooting area / total sample area (%)	0.023	0.011	0.013	0.008	0.005

* *Corresponding author address:* Chuntao Liu, Univ. of Utah, Dept. of Meteorology, Salt Lake City, UT, 84112; e-mail: *liuct@met.utah.edu*

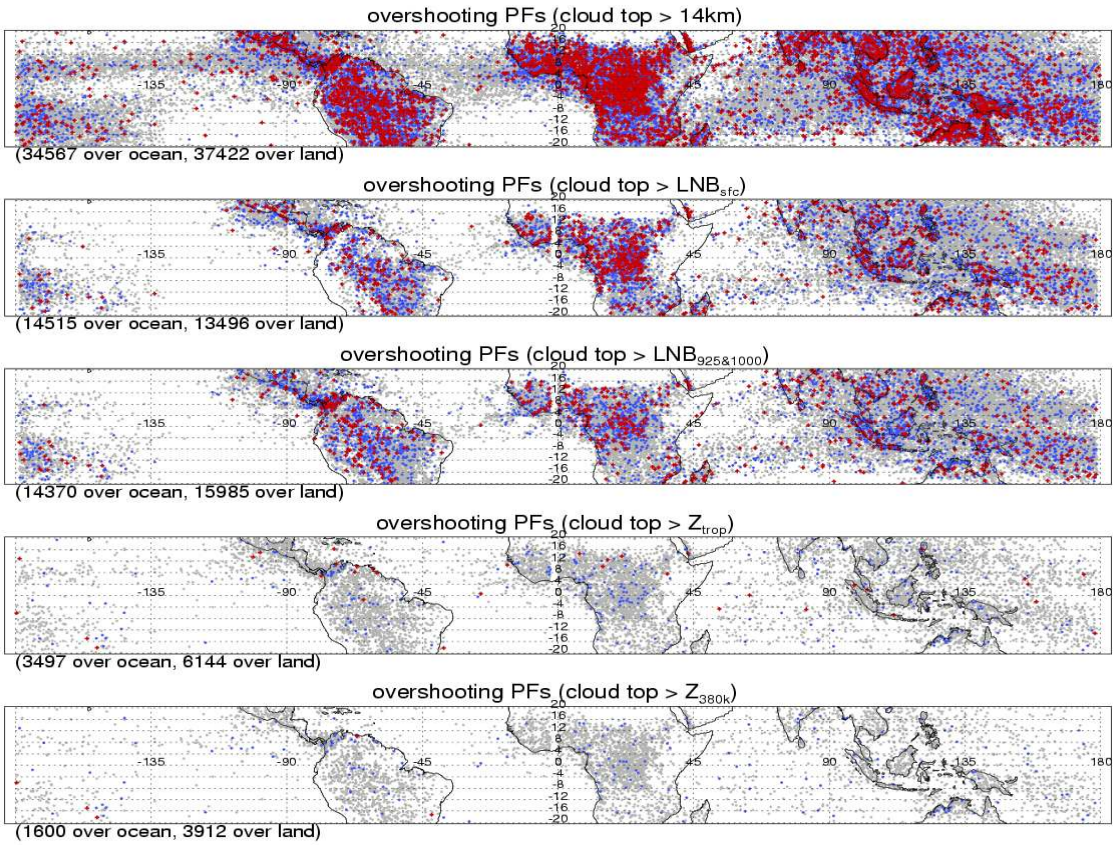

Figure 1. Location of identified overshooting PFs at 20°N-20°S using different reference heights. The PFs with overshooting distance greater than 2 km are in blue, greater than 3 km are in red.

3. RESULTS AND DISCUSSION

In this section, the global distribution, seasonal, diurnal variation and the properties of these OPFs are discussed.

3.1 Global distribution of population of OPFs

Figure 1 demonstrates the locations of PFs penetrating different reference heights. A similar geo location distribution pattern exists for all 5 groups: OPFs were found mainly over the West Pacific, Central Africa, South America, ITCZ and SPCZ. The overshooting tops above 17 km (red dots in the top panel of Figure 1) occur mainly over land. About the same number of PFs above 14 km cloud top were found over land and ocean. But more land PFs were capable of penetrating the higher reference heights (Z_{380K} and $Z_{tropopause}$). There is less strong overshoot activity in the ITCZ regions of the East Pacific and Atlantic. Two regions were found with frequent, strong overshooting activity: The Congo basin and Panama. Over the West Pacific region (Maritime Continent), strong overshooting was observed mostly over the land portion of that box.

3.2 Size and overshooting area percentage of OPFs

Since overshooting convection may play an important role on the troposphere-stratosphere mass exchange, information of overshooting area and size of OPFs is tabulated. The histogram of overshooting area and horizontal size is generated in Figure 2. From Table 1, only 0.18% of the cloudy area is found above the tropical tropopause. However, this does not mean that every convective system has a small overshooting area. As shown in Figure 2, there are PFs with overshooting area above the tropopause up to 5000 km^2. Most land OPFs penetrating Z_{trop} have horizontal size about ~1000km^2 and ~20% overshooting area. Most oceanic OPFs with tops higher than Z_{trop} have a relatively larger size and smaller overshooting area than those over land. This leads to the larger overshooting area percentage for land OPFs. The OPFs with extremely high overshooting area percentage, for example, with >40%, were only found over Africa, South America during all seasons and over Darwin during southern summer. On the other hand, there are many oceanic OPFs with huge size found over the west Pacific, which rarely happened over land (figure not shown). A similar pattern was found for OPFs from other reference heights and is not shown here.

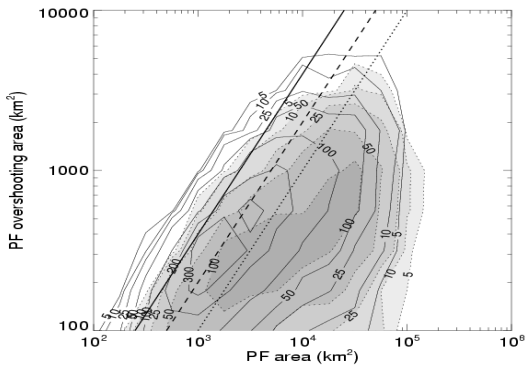

Figure 2. Number density histogram of area and overshooting area of OPFs (20°N-20°S) with cloud top above Z_{trop} over land (solid contours) and over ocean (shaded with dash contours). The 10% (dot line), 20% (dash line) and 40% (solid line) area percentage line are overlapped.

3.3 Global distribution of tropical overshooting area, volume and precipitating ice mass

To show the global distribution of overshooting area above each reference height, the overshooting area from each OPF is accumulated in 5°x5° boxes. The count of TRMM 3A25 total PR pixels is used to remove the sampling bias. After weighting by the total overshooting area, the global distribution of overshooting is obtained and shown in Figure 3. The global distribution of overshooting area from OPFs with different reference heights shows a very similar pattern. The overshooting is not randomly distributed, but concentrates in specific regions, notably the Congo Basin, Panama, Columbia, Indonesia, Malaysia and Northern Australia. Congo Basin and Panama are the most active regions. The global distribution of tropical overshooting volume and precipitating ice mass are generated using similar methods. The distributions of volume and precipitating ice mass demonstrate an almost identical pattern as that of Figure 3 (not shown).

In order to demonstrate the contribution of overshooting from different parts of the tropics, the latitude belt from 20°N-20°S is divided into 8 equal-area regions as shown in Figure 3e. The total contributions of OPF numbers and overshooting area, volume and precipitating ice mass over each region, as well as over land and ocean, are calculated and listed in Table 2. Between 20°N-20°S, only 23% of the area is land, 77% ocean. However, more than half of OPFs above 14 km and their overshooting area, volume and precipitating ice mass were found over land. This land domination is stronger when higher reference heights are used. About 73% of the overshooting area and volume above the 380 K level are over land. The contribution of overshooting area, volume and precipitating ice mass

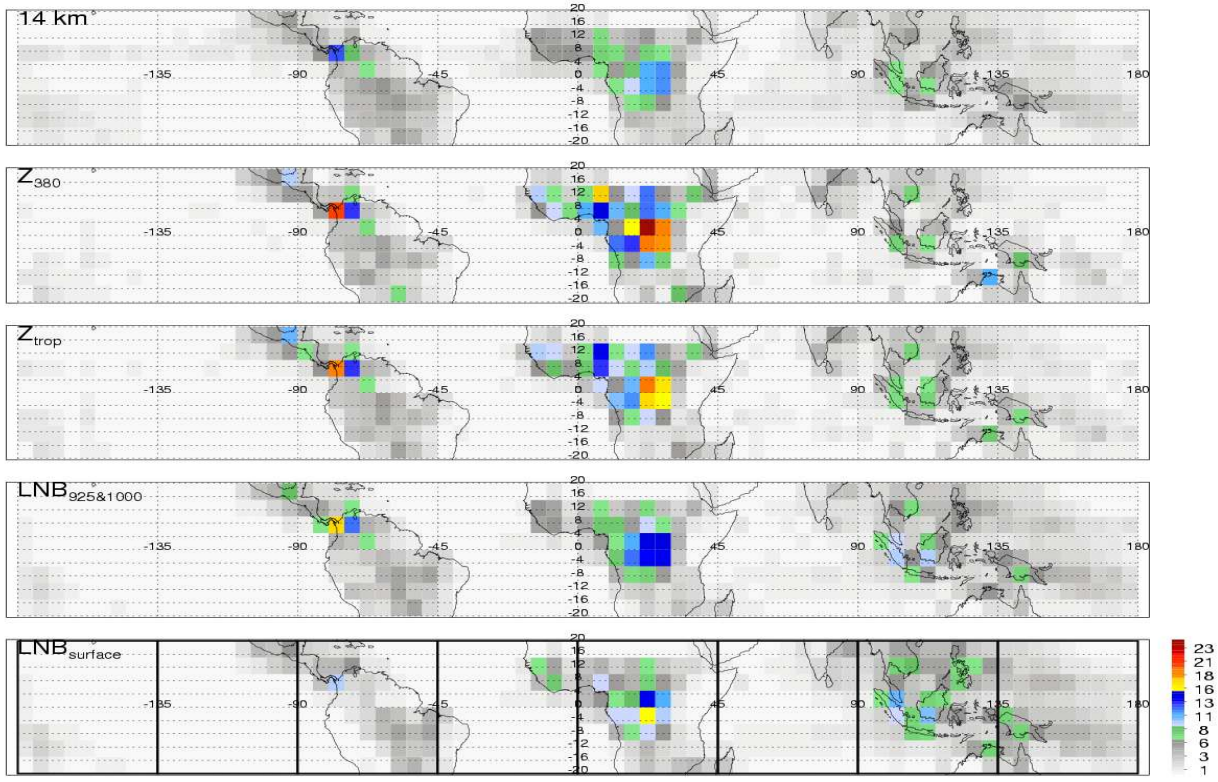

Figure 3. Global distribution of overshooting area contribution in 5°x5° boxes from OPFs above different reference heights (in units ‰). The distribution is normalized with TRMM 3A25 total pixel number to remove the sampling bias.

Table 2. Global distribution (in units %) of tropical OPF population and overshooting area, volume and precipitating ice mass using different reference heights.

	Reference heights	180°W – 135°W	135°W – 90°W	90°W – 45°W	45°W – 0°	0° – 45°E	45°E – 90°E	90°E – 135°E	135°E – 180°E	Land	Ocean
Num	14 km	5.9	4.6	20.2	5.7	19.0	7.3	20.8	16.5	51.7	48.3
	LNB_{sfc}	6.5	5.0	21.9	5.6	20.1	7.7	18.4	14.7	53.2	46.8
	$LNB_{925\&1000}$	7.5	5.4	22.0	5.9	16.2	8.5	18.7	15.9	47.9	52.1
	Z_{trop}	3.3	4.1	21.5	7.8	22.7	5.1	21.8	13.8	62.0	37.0
	Z_{380K}	3.0	4.3	21.0	5.5	31.7	6.2	18.1	10.3	70.1	29.9
Area	14 km	4.8	4.7	19.4	6.7	25.5	7.0	19.2	12.7	58.1	41.9
	LNB_{sfc}	5.0	4.9	20.2	6.1	26.4	7.2	18.2	12.1	58.7	41.3
	$LNB_{925\&1000}$	5.5	5.1	20.4	6.4	24.1	7.6	18.4	12.6	55.4	44.6
	Z_{trop}	2.7	4.1	19.1	8.0	30.9	5.8	19.1	10.2	66.9	33.1
	Z_{380K}	2.2	4.3	17.8	6.2	38.5	6.3	16.7	7.9	72.9	27.1
Volume	14 km	4.2	4.2	18.8	6.4	26.4	6.8	20.1	13.0	60.1	39.9
	LNB_{sfc}	4.4	4.4	19.4	5.8	27.2	7.0	19.4	12.5	60.5	39.5
	$LNB_{925\&1000}$	4.7	4.5	19.6	6.0	25.4	7.3	19.6	12.9	58.1	41.9
	Z_{trop}	2.5	3.8	18.5	7.5	31.5	6.0	19.9	10.4	68.3	31.7
	Z_{380K}	2.1	4.0	17.3	6.0	38.1	6.3	17.9	8.4	73.4	26.6
Mass	14 km	3.0	3.7	18.8	7.1	32.8	6.4	18.3	10.0	69.2	30.8
	LNB_{sfc}	3.0	3.8	19.2	6.3	33.6	6.5	18.0	9.7	69.5	30.5
	$LNB_{925\&1000}$	3.2	3.9	19.4	6.4	32.3	6.7	18.1	9.9	68.0	32.0
	Z_{trop}	1.6	3.4	18.1	8.3	37.8	5.8	17.5	7.6	76.5	23.5
	Z_{380K}	1.2	3.5	16.8	6.8	43.5	6.2	16.0	6.1	80.5	19.5

from 0°-45°E (including Africa) is the largest among the 8 regions. The contribution from Africa alone is greater than the total contributions from Central and East Pacific (180°W-90°W), Atlantic (45°W-0°) and Indian (45°E-90°E) Oceans combined. South America and the West Pacific also contribute significant overshooting areas, although the contribution from the west Pacific is mainly from the land areas of the Maritime continent (Figure 3).

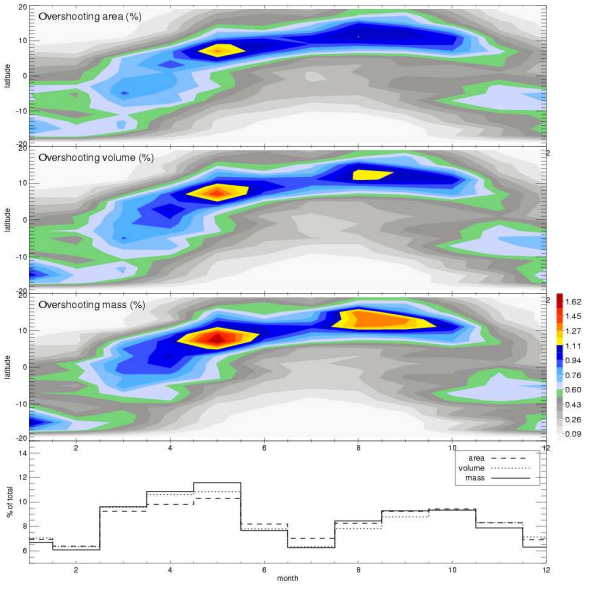

Figure 4. Seasonal and latitudinal distribution of contribution of overshooting area, volume and precipitating ice mass from the OPFs above 14 km (in units %). The contribution contour is generated with 1 month and 2° intervals.

3.4 Seasonal variation of tropical overshooting area, volume and precipitating ice mass

The global distributions of tropical overshooting area at different seasons are analyzed using the same method as in Figure 3. To demonstrate the seasonal variation of total overshooting area, volume and precipitating ice mass, these overshooting properties are integrated with 2° latitude intervals for each month. After removing the sampling bias with TRMM 3A25 total pixels, the percentage of overshooting contribution at each 2° latitude region in each month is calculated by weighting the total amount of overshooting area, volume and precipitating ice mass respectively. As shown in Figure 4, there are two main overshooting seasons in the Northern tropics, May, and Aug-Oct., which lead to a semi annual cycle of overshooting area, volume and precipitating ice mass. A similar pattern is found for OPFs defined with other reference heights (not shown).

3.5 Thermodynamic environment of overshooting storms

To investigate why overshooting are stronger over Africa and South America than over oceans, the global distribution of mean Convective Available Potential Energy (CAPE) is analyzed using 5 years of NCEP reanalysis data (Figure 5). Africa, Panama and islands of the Maritime Continent have higher mean CAPE than South America and Tropical Oceans. The Cumulative Distribution Functions (CDF) of CAPE in the selected regions (from Figure 5) during the convection active seasons are shown in Figure 6. MAM and SON Congo have higher CAPE than any other area. The weakest CAPE is found over JJA East Pacific and Tropical Atlantic (GATE area). These patterns seem to be

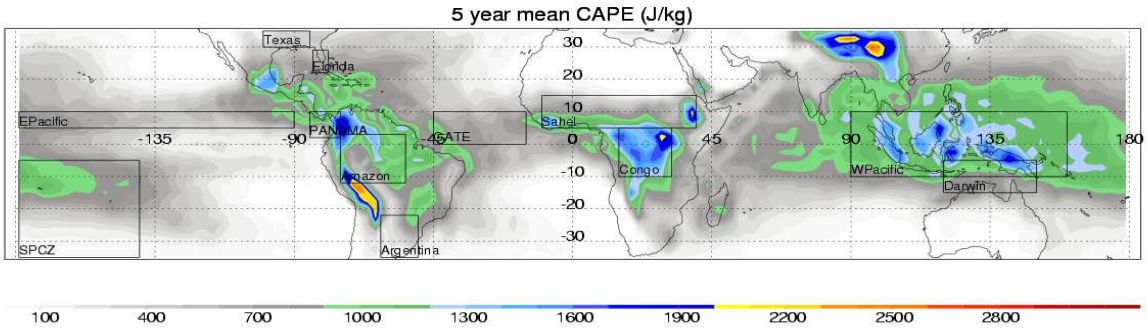

Figure 5. Global distribution of mean CAPE calculated from 5 year NCEP reanalysis data.

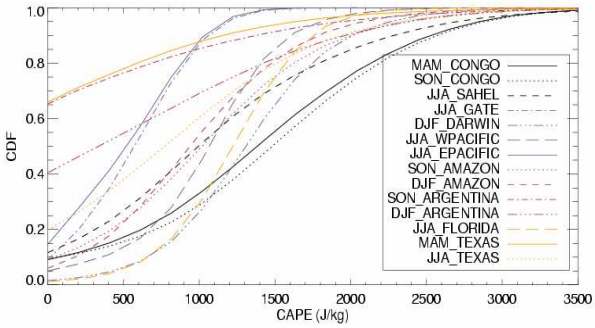

Figure 6. Cumulative distribution function CDF) of CAPE in the selected regions during the most active convection season for each region.

consistent with the overshooting active regions. However, *this does not mean that CAPE may be used as a good indicator for the OPFs*. As shown in Figure 7, only Congo has higher CAPE in OPFs than the average. Other regions do not show any trend of high CAPE in OPFs. CAPE in OPFs over the West Pacific tends to be even smaller than the average. Due to low horizontal, and vertical resolution of the NCEP reanalysis data, CAPE values shown here may have large errors. Thus, much more investigation is needed to explain these results for geographical distribution of intense storms.

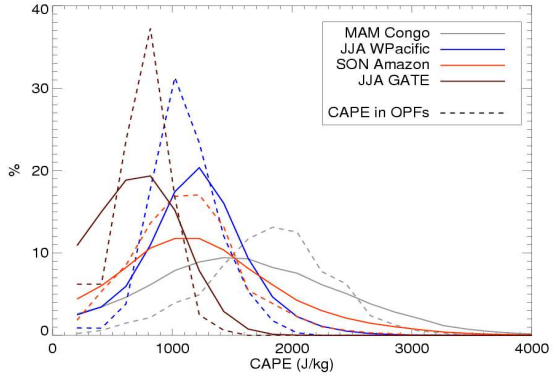

Figure 7. Histogram of CAPE over selected region (solid lines) and the CAPE in the OPFs above 14 km (dash lines).

3.6 Implications of observed overshooting properties

The overshooting area, volume and mass shown in this study only apply *directly* to precipitating ice particles with 20 dBZ echoes above the reference heights in convection. Most likely these particles would fall out of the TTL in a short time [Alcala and Dessler, 2002]. A major question that we cannot answer at this time is the relationship between what we *can* measure with the TRMM PR, and what we *cannot* measure. What is the relationship between the precipitating ice mass, and the mass of small ice particles which accompany the larger particles in intense convective overshooting towers? These small ice particles fall slowly and may remain aloft for a long time, and may evaporate at unknown altitudes within the TTL. To relate the overshooting air and ice mass to the troposphere and stratosphere mass exchange, it is necessary to know how much air and ice mass would remain in the TTL. However, the mixing and detrainment of air and ice mass from the overshooting cloud tops to the environment in the TTL is a complicated process and still under investigation [Sherwood and Dessler, 2003]. This limits our ability to relate our results to the troposphere-stratosphere transport problem.

However, it may be reasonable to speculate that there is a positive relationship between the TRMM-detected overshooting area and the amount of air and mass of small ice particles injected into TTL by intense convection. If so, the global distribution of overshooting area found in this study may represent the distribution of air colder and dryer than the environment TTL. In that case, the results in this study may lead to a contradiction. Some studies suggest that the deep convection has an important impact on the water vapor budget [Sherwood and Dessler, 2000]. From this study, it is hard to use the semi annual cycle of the deep convection overshooting area to explain the well known annual cycle of water vapor in the low stratosphere [McCormick et al., 1993]. Thus, the clarification of the relationship between the mass of large ice particles and the mass of small ice particles in the overshooting tops, and the rate of mixing and detraining of air and ice mass from overshooting tops to the TTL environment demands further study.

4. SUMMARY

Five groups of tropical deep convection with overshooting tops are identified using 5 different reference heights and a 5-year TRMM database of precipitation features. The common properties of these extreme convective systems are examined from a global perspective. It is found that 1% of deep convective systems reach 14 km and 0.1% of them may even penetrate the 380K potential temperature level. A high population of overshooting deep convection over Africa is found during all the seasons. Stronger overshooting convection is found over land, especially central Africa, South America and the large islands of the Indonesian region. Overshooting area and the relative percentage for convective systems over land tend to be larger than that over ocean. There is a large seasonal variation of overshooting over South America. The largest contribution of overshooting area, volume and precipitating ice mass is found from convection over central Africa. There is a semi annual cycle in the total overshooting area, volume and precipitating ice mass over the tropics as a whole. The seasonal and geo-distribution patterns show a good consistency among the 5 groups of overshooting deep convection, differently defined. Global distribution of CAPE calculated from NCEP reanalysis data is basically consistent with overshooting active regions. However, NCEP CAPE is generally not a good indicator for the location and timing of the overshooting storms. This may due to the uncertainty of the CAPE estimation from low horizontal and vertical resolution NCEP reanalysis data. It may also reflect the reality that large CAPE alone is a necessary but not sufficient condition for intense convective storms.

Acknowledgements. This work was supported by the NASA TRMM office under grant NAG5-13628. The data were processed by the TRMM Science Data and Information System (TSDIS).

References

Alcala, C. M. and A. E. Dessler, 2002: Observations of deep convection in the tropics using the tropical rainfall measuring (TRMM) precipitation radar, *J. Geophys. Res.*, 107, doi:10.1029/2002JD002457.

Carey, L. D., and S. A. Rutledge, 2000: The relationship between precipitation and lightning in tropical island convection: a c-band polarimetric radar study, *Mon. Weather Rev.*, 128, 2687-2710.

Gettelman, A., M. L. Salby, and F. Sassi, Distribution and influence of convection in the tropical tropopause region, *J. Geophys. Res.*, 107, doi:10.1029/2001JD001048, 2002.

Kistler, R., E. Kalnay, W. Collins, S. Saha, G. White, J. Woollen, M. Chelliah, W. Ebisuzaki, M. Kanamitsu, V. Kousky, H. Dool, R. Jenne, and M. Fiorino, The NCEP-NCAR 50-year reanalysis: monthly means CD–ROM and documentation, *Bull. Am. Meteorol. Soc.*, 82, 247-267, 2001.

Kummerow, C., and W. Barnes, The tropical rainfall measuring mission (TRMM) sensor package, *J. Atmos. Oceanic Technol.*, 15, 809-817, 1998.

McCormick, M. P., E. W. Chiou, L. R. McMaster, W. P. Chu, J. C. Larsen, D. Rind, and S. Oltmans, Annual variation of water vapor in the stratosphere and upper troposphere observed by the Stratospheric Aerosol and Gas Experiment II, *J. Geophys. Res.*, 98, 4867-4874, 1993.

Nesbitt, S. W., E. J. Zipser, and D. J. Cecil, A census of precipitation features in the tropics using TRMM: radar, ice scattering, and lightning observations, *J. Clim.*, 13, 4087-4106, 2000.

Sherwood, S. C., and A. E. Dessler, On the control of stratospheric humidity, *Geophys. Res. Lett.*, 27, 2513-2516, 2000.

--, --, Convective mixing near the tropical tropopause: insights from seasonal variations, *J. Atmos. Sci.*, 60, 2674-2685, 2003.

Simpson, J., R. F. Adler, and G. R. North, A proposed tropical rainfall measuring mission (TRMM) satellite**,** *Bull. Am. Meteorol. Soc.*, 69, 278-295, 1988.

Spencer, R. W., H. G. Goodman, and R. E. Hood, Precipitation retrieval over land and ocean with the SSM/I: identification and characteristics of the scattering signal, *J. Atmos. Oceanic Technol.*, 6, 254-273, 1989.